

Semblance study of force-field and convection-diffusion solutions with observations of solar magnetic phenomena

M. ENRÍQUEZ-VARGAS¹ AND JORGE U. PÉREZ ROMERO²

¹*Instituto de Astronomía, Universidad Nacional Autónoma de México,
04510, Ciudad de México, México*

²*Facultad de Ingeniería, Universidad Nacional Autónoma de México,
04510, Ciudad de México, México*

ABSTRACT

We propose a quantitative model using the semblance method to evaluate differences in transport equation solutions and Local Interstellar Spectra (LIS) for Cosmic Ray (CR) modulation. The semblance method quantitatively compares transport solutions—convection-diffusion and force field—and LIS, providing insights into CR behavior.

By integrating these solutions into the atmospheric yield function (Caballero-Lopez & Moraal 2012), the model identifies a correlation between the modulation factor and sunspots, and an anti-correlation with the mean magnetic field. The force field solution shows stronger semblance values, aligning better with neutron detector data. Among LIS, models by Lagner, Potgieter & Webber (2003), and Ghelfi et al. (2017) are most consistent, while the Garcia-Munoz et al. (1975) LIS reveals notable variations.

This study underscores the semblance method as a critical tool for comparing CR modulation models, advancing predictive models of cosmic ray behavior influenced by solar and interstellar conditions.

Keywords: Cosmic Rays — Convection-Diffusion solution — Force field solution — Semblance — Geophysics — Local interstellar spectral — Atmospheric yield function

1. INTRODUCTION

To generate the proposed model, data from neutron monitors were utilized and diverse local interstellar spectra were computed. These spectra were introduced into the atmospheric yield function to determine the cosmic ray modulation factor.

Primary cosmic rays are electrically charged particles and sometimes can reach velocities as high as the speed of light. Primary cosmic radiation is composed of protons, α -particles (two protons and two neutrons), ${}^4\text{He}$ and heavy nuclei.

Primary cosmic rays enter the Earth's magnetosphere and interact with the particles in the Earth's atmosphere, those violent collisions produce smaller particles (secondary cosmic rays). This process is repeated multiple times until the particles lose sufficient energy to become elemental particles or are unable to break down

due to energy loss. This phenomenon is known as an air shower (Auger et al. 1939).

High-energy cosmic rays are produced by stochastic collisions within a magnetically turbulent plasma such as a supernova, however there are also low-energy cosmic rays from similar stars to our Sun (Sekido & Elliot 1985).

Cosmic rays originating from sources beyond our solar system are detected on Earth's surface, and their detection is affected by solar activity, which is reliant on the solar cycles. Furthermore, the Sun also generates cosmic rays within its atmosphere.

The semblance method has been used to compute the desired model. Semblance is a geophysical tool mainly used in exploration seismology, and it can be defined as a correlation in Fourier terms or other transforms between two traces, that is, semblance is a measure to compute the similarity between two traces.

2. TRANSPORT EQUATION

The solutions of the transport equation used in this document are based on Caballero-Lopez and Moraal (Caballero-Lopez & Moraal 2004) article.

¹ Computational resources can be found in <https://github.com/JorUrie/TRC.git>

The Parker's equation is given by:

$$\frac{\partial f}{\partial t} + \frac{1}{4\pi p^2} \nabla \cdot \vec{S} + \frac{1}{p^2} \frac{\partial}{\partial p} (p^2 \dot{p}) f = Q \quad (1)$$

where S is the current differential density:

$$\vec{S} = 4\pi p^2 (C \vec{V} f - K \cdot \nabla f) \quad (2)$$

The equation 1 is in terms of the omnidirectional distribution function $f(r; P; t)$, where p is the moment of the particle, t is the time, r is the radial distance, Q is the source of cosmic rays and V the solar wind speed. K is the diffusion tensor, that contains a parallel component k_{\parallel} , perpendicular k_{\perp} and transverse k_T , and they describe the drifts. In the equation 2, C (from the equation 3) is known as the Compton-Getting factor (Gleeson & Axford 1968). This factor was introduced into the transport equation, because the flow is isotropic in the reference system at rest and is not the same in the solar wind system.

$$C = -\frac{1}{3} \frac{\partial \ln f}{\partial \ln p} \quad (3)$$

The adiabatic energy loss is denoted as:

$$\dot{p} = -\frac{p}{3} \nabla \cdot \vec{V} \quad (4)$$

Substituting 3 and 4 into 1 two possible solutions could be obtained:

$$\frac{\partial f}{\partial t} + \nabla \cdot \underbrace{(C \vec{V} f - K \cdot \nabla f)}_a + \underbrace{\frac{1}{p^2} \frac{\partial}{\partial p} \left[p^2 \left(\frac{p}{3} \vec{V} \cdot \frac{\nabla f}{f} \right) \right]}_c f = Q \quad (5)$$

3. FORCE FIELD

In equation 5 the term a corresponds to the convection, b to the diffusion and drifts of the cosmic rays, and c to the changes in energy. To solve the previous equation, different conditions have been considered. If a steady state, no sources, and negligible energy losses are assumed, the following can be obtained from equation 5:

$$CVf - K \cdot \nabla f = cnst. = 0 \quad (6)$$

Equation 6 is valid when the term for adiabatic losses in equation 7 is smaller than the terms convective and diffusive:

- $Vr = k \ll 1$ valid for high energy cosmic rays, since k is proportional to energy.
- $(1/f) \partial f / \partial r \ll C/r$ valid for small r , that is, in the internal heliosphere.

Considering spherical symmetry, 8 is:

$$CVf - k \frac{\partial f}{\partial r} = 0 \quad (7)$$

The force field equation in terms of rigidity and knowing that $P = cp/q$:

$$\frac{\partial f}{\partial r} + \frac{VP}{3k} \frac{\partial f}{\partial P} = 0 \quad (8)$$

From:

$$df(r, P) = \frac{\partial f}{\partial r} dr + \frac{\partial f}{\partial P} dP \quad (9)$$

dividing by dr :

$$\frac{df}{dr} = \frac{\partial f}{\partial r} + \frac{\partial f}{\partial P} \frac{dP}{dr} \quad (10)$$

Considering the equation 8:

$$df = 0 \quad (11)$$

Equation 11 implies that $f(r, p)$ is constant, equal to its value at the boundary, along a contour with characteristic equation $dP/dr = VP/3k$, in the space (r, P) . In the second term of the equation 8, the quantity VP/k has units of potential per unit length, that is, force units, this is why it is called a force field solution. Considering the diffusion coefficient with the form:

$$k(r, P) = \beta k_1(r) k_2(P) \quad (12)$$

the solution of the characteristic equation remains as:

$$\int_P^{P_b(r, P)} \frac{\beta(P') k_2(P')}{P'} dP' = \int_r^{r_b} \frac{V(r')}{3k_1(r')} dr' \equiv \phi(r) \quad (13)$$

where ϕ is the force field parameter. When $k_2 \propto P$ and $\beta \approx 1$, the solution is reduced to the most commonly used form:

$$\phi = P_b - P \quad (14)$$

4. CONVECTION-DIFFUSION

From equation 5, Q is not the adiabatic loss in a rest system:

$$Vf - k \frac{\partial f}{\partial r} = 0 \quad (15)$$

The outcome is:

$$f = f_b e^{-M} \quad (16)$$

Where $M = \int_r^{r_b} \frac{V dr}{k}$ is the modulation function, ϕ is the force field parameter. Its outcome is:

$$M = \frac{3\phi}{\beta k_2} \quad (17)$$

Where M does not have units.

Both solutions are introduced into the atmospheric yield solution, which is necessary to compute the modulation factor. However, LIS is also necessary in order to compute the atmospheric yield solution.

5. LOCAL INTERSTELLAR SPECTRAL

The Local Interstellar Spectrum is a mathematical model created from observations or simulations and describe the arrival of the Cosmic Rays outside the Heliosphere in energy terms.

The LIS models used in these analyses were Lagner, Potgieter & Webber LIS in 2003, Burguer & Potgieter LIS in 2000, Garcia-Munoz, Mason & Simpson LIS in 1975 and Ghelfi, Barao, Derome & Maurin LIS in 2017.

5.1. *Lagner, Potgieter & Webber LIS in 2003*

This LIS is based on an analytic solution of the Parker equation (Parker 1965), using Voyager 1, Voyager 2 and Pioneer data at 70 Astronomical Units (AU) close to the Terminal Shock (TS) during the solar minimum between 1987 and 1997.

The modulation developed by Parker included drift effects which are related to the polarity of solar magnetic field:

$$\frac{\partial f}{\partial t} = - (V + \langle v_D \rangle) \cdot \nabla f + \nabla \cdot (K_S \cdot \nabla f) + \frac{1}{3} (\nabla \cdot V) \frac{\partial f}{\partial \ln P} + j_{source} \quad (18)$$

Where j_{source} is the local source. In the equation, parallel, perpendicular, and asymmetric drift coefficients were introduced to describe the gradients and drifts of curvature in large-scale Heliospheric Magnetic Field (HMF).

The local sources are not considered and are time-dependent in a spherical coordinate system modeled as a combination of diffusive shock acceleration and drift modulation in two spatial dimensions, neglecting any azimuthal dependence and assuming a symmetrical equatorial field (Langner et al. 2003). The model offers several CR intensities, which are interpreted as particles of different compositions. When the modulation is computed close to or outside the TS, it shall be computed in rigidity terms. The protons model is the following:

$$J_H = \frac{2.1 E_k^{-2.8}}{1 + 5.85 E_k^{-1.2} + 1.18 E_k^{-2.54}} \quad (19)$$

And the Helium model is:

$$J_{He} = \frac{1.075 E_k^{-2.8}}{1 + 3.9 E_k^{-1.09} + 0.90 E_k^{-2.54}} \quad (20)$$

5.2. *Burguer & Potgieter LIS in 2000*

The LIS was compared to ULYSSES data from September 1994 to July 1995 with a Fast Scanning of Latitude (FSL). The Parker equation was analytically solved considering an omnidirectional distribution (two dimensions), the source is located 100 UA, the velocity of the Solar Wind (SW) is $400 \frac{km}{s}$ in equatorial plane, and it is increasing to $800 \frac{km}{s}$ in polar zones. The HMF angle sheet is 15° , which is a good value to fit for solar modulation. The model was computed by Bibber (Bieber 1999):

$$f_{IS}(R) = \begin{cases} 1.9 \times 10^4 R^{-2.78} & \text{If } R \geq 7GV \\ \exp(9.472 - 1.999R - 0.6938R^2 + 0.2988R^3 - 0.04714R^4) & \text{If } R < 7GV \end{cases} \quad (21)$$

The model can also be expressed in terms of proton composition:

$$J_H = \frac{1.9 \times 10^4 P^{-2.78}}{1 + 0.4866 P^{-2.51}} \quad (22)$$

$$J_{He} = \frac{(3.8 \times 10^4 P^{-2.78})}{(1 + 0.9732 P^{-2.51})} \quad (23)$$

5.3. *Garcia-Munoz, Mason and Simpson LIS in 1975*

To compute this LIS, IMP-5, IMP-7, and IMP-8 data were consulted, because the satellites can capture several particles and their energy range is the widest. The selected data were electrons $> 100 MeV$ with quiet-time measurements.

The Parker's equation was analytically solved considering a symmetric spherical coordinate system in steady state and drawing on Fisk's method (Fisk et al. 1974). The LIS is the following:

$$j = A(T + B \exp(-CT))^\gamma \quad (24)$$

Where j is particle flux, T is kinetic energy and parameters are shown in Table 1:

Species	A	B	C	γ
H	9.9×10^8	780	2.5×10^{-4}	2.65
4He	1.4×10^8	660	1.4×10^{-4}	2.77
C	1.8×10^6	620	5.2×10^{-4}	2.68

Table 1: Equation 7 parameters Garcia-Munoz et al. (1975)

5.4. *Ghelfi, Barao, Derome and Maurin LIS in 2017*

The data used were AMS-01 and AMS-02, BESS-Polar and PAMELA, because they were recent (at that time), but Voyager 1 data was also considered.

First, the author proposes the simplest modulation model to link unmodulated (IS) to modulated (TOA) quantities, which is a force field approximation Ghelfi et al. (2017):

$$\frac{E^{TOA}}{A} = \frac{E^{IS}}{A} - \frac{|Z|}{A} \phi \quad (25)$$

$$J^{TOA}(E^{TOA}) = \left(\frac{p^{TOA}}{p^{IS}} \right)^2 \times J^{IS}(E^{IS}) \quad (26)$$

Where E is total energy, p is the momentum, and $J \equiv \frac{dJ}{dE_k^n}$ is the differential flux per kinetic energy per nucleon E_k^n .

An analysis χ^2 was necessary to fix the TOA flux with all the species $N_j(i)$ in this t_j , over all possible energy $E_k(i, j)$ and is given by:

$$\chi^2 = \sum_{t_i} \sum_{N_j(i)} \sum_{E_k(i,j)} \frac{(J^{TOA}(J_j^{IS}, \phi_j, E_k) - data_{ijk})^2}{\sigma_{ijk}} \quad (27)$$

Where IS parameters are free. For the previously mentioned cases, power laws in total energy (O'Neill 2006) or rigidity (Shikaze et al. 2007). TOA data for H and He are

old and have more inconsistencies than new data, thus, a χ^2 analysis was applied to minimize errors. Therefore, the MINUIT minimization package was used (James 1998) from Root CERN libraries Sartini et al. (2010). Markov Chain Monte Carlo analysis (MCMC) was implemented from the GreAT package (Putze & Derome 2014) to determine the correlation between credible intervals for ϕ and IS flux. MCMC analysis is based on Bayes' theorem. Finally, all the obtained data is represented as an interpolation of logarithmic-polynomial functions, as shown in equation 28.

$$\log_{10}(J_{IS}) = \begin{cases} \sum_{i=0}^{12} c_i \left(\frac{\log_{10}\left(\frac{E_{\frac{k}{n}}}{800 \frac{GeV}{n}}\right)}{\log_{10}\left(\frac{E_{\frac{k}{n}}}{800 \frac{GeV}{n}}\right)} \right)^i & \text{if } E_{\frac{k}{n}} < 800 \frac{GeV}{n} \\ C_0 - C_1 \left(\frac{\log_{10}\left(\frac{E_{\frac{k}{n}}}{800 \frac{GeV}{n}}\right)}{\log_{10}\left(\frac{E_{\frac{k}{n}}}{800 \frac{GeV}{n}}\right)} \right) & \text{if } E_{\frac{k}{n}} \geq 800 \frac{GeV}{n} \end{cases} \quad (28)$$

In this paper, just four LIS were applied, however more models were also considered, and it is worthwhile to mention them.

5.5. *Boschini, Della Torre, Gervasi and more LIS in 2018*

For the calculation of this LIS the GALPROP and HelMod programs were used to simulate CR data, but real data was required, so Voyager 1, BESS, PAMELA, AMS-01 and AMS-02 data were consulted.

The GALPROP code uses astronomical, particle physics and nuclear information to predict CR flux, X-ray, synchrotron emissions and their polarization (Strong et al. 2007). Heliosphere propagation was computed by GALPROP and thanks to the MCMC analysis, the data became more realistic. Afterward, the information was introduced into the HelMod program to obtain modulated data.

Previous data was compared with real information from the satellites with different energy content. The used information was a combination of Voyager 1, AMS-02, CREAM-I and ATIC-02, but CREAM-I and AMS-02, because they had better adjustments and offered minimal errors. To compute the analytical LIS, MCMC analysis from Eureqa¹ was used, the outcome is given:

$$F(R) \times R^{2.7} = \begin{cases} \sum_{i=0}^5 a_i R^i & R \leq 1GV \\ b + \frac{c}{R} + \frac{(d_1)}{d_2+R} + \frac{(e_1)}{e_2+R} + \frac{(f_1)}{f_2+R} + gR & R \geq 1GV \end{cases} \quad (29)$$

Where the parameters are showing in the table 2.

	a_0	a_1	a_2	a_3	a_4	a_5	b	c	d_1	d_2	e_1	e_2	f_1	f_2	g
p	91.1	-831	0	16700	-10200	0	10800	8590	-4230000	3190	274000	17.4	-39400	0.464	0
H	1.14	0	-118	578	0	-87	3120	-5530	3370	1.29	134000	88.5	-1170000	861	0.03

Table 2. Equation 12 parameters (Boschini et al. 2017)

¹ <http://www.nutonian.com/products/eureqa/>

5.6. *Vos & Potgieter LIS in 2015*

The LIS was computed using observations from PAMELA data during a solar minimum from 2006 to 2009. This LIS was computed from the Parker equation (Parker 1965), which was solved as a ray distribution function in rigidity terms, time, position in 3D, in heliocentric spherical coordinates where the polar angle is equal to 90°. All short-term modulation effects were neglected (solar minimum conditions). The average particle drift velocity is caused by gradients and curvature in Heliospheric Magnetic Field (HMF), there is a symmetric diffusion tensor and adiabatic energy changes except in the heliosheath (Potgieter et al. 2012).

The LIS is the following (Vos & Potgieter 2015):

$$j_{LIS} = 2.70 \left(\frac{E^{1.12}}{\beta^2} \right) \left(\frac{E + 0.67}{1.67} \right)^{-3.93} \quad (30)$$

Where E is kinetic energy, $\beta = \frac{v}{c}$ particle velocity (like light velocity), $j_{LIS} = P^2 f$.

5.7. *Moskalenko, Strong, Ormes and Potgieter LIS in 2002*

The cosmic ray data was simulated using the DTUNUC Monte Carlo code (Ferrari et al. 1996), and additional data was collected from two previous works (Tan & Ng 1983). The Parker equation (Parker 1965) was solved through Crank-Nicholson numerical solution (Crank & Nicolson 1947) and according to the author: a more realistic model was sought. Thus, the leaky box code (weighted-slab) was applied. GALPROP was also used to compute 3D cosmic rays.

The Helium LIS was approximated using a force field solution due to the low-energy approximation, and the ϕ potential modulation was selected using the CLIMAX neutron monitor.

To ensure that the spectrum is similar to the simulated values, a power law dependent on kinetic energy based on the convection-diffusion solution has been approximated, which cannot only be described by a single function.

Finally, the LIS was subjected to a χ_n^2 function to observe the quality of the adjusted data for each individual measurement (Moskalenko et al. 2002) as shown in equation 31:

$$J_H = \begin{cases} \exp \left(4.64 - 0.08 \left(\log \left(\frac{E_{\frac{k}{n}}}{1 GeV} \right) \right)^2 - 2.91 \sqrt{\frac{E_{\frac{k}{n}}}{1 GeV}} \right), & E_{\frac{k}{n}} \leq 1 GeV \\ \exp \left(3.22 - 2.86 \log \left(\frac{E_{\frac{k}{n}}}{1 GeV} \right) - \frac{1.5}{E_{\frac{k}{n}}} \right), & E_{\frac{k}{n}} > 1 GeV \end{cases} \quad (31)$$

The previously mentioned LIS are shown in the figure 2 using the rigidity-purpose parameters defined by each author:

6. SEMBLANCE

The semblance is the cross-relation between two traces, the computed value is interpreted as the similarity of two points contained in the traces within the Fourier domain. However,

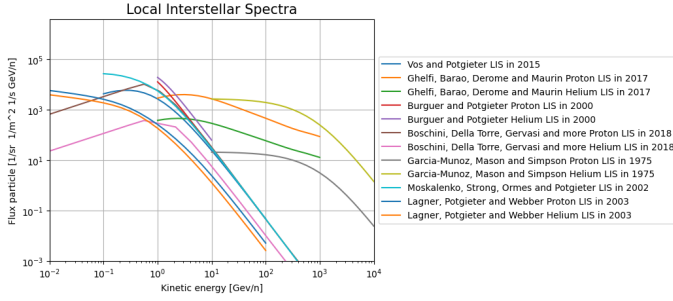


Figure 2: Local Interstellar Spectral purpose by (Vos & Potgieter 2015), (Ghelfi et al. 2017), (Burger et al. 2000), (Boschini et al. 2017), (Garcia-Munoz et al. 1975), (Moskalenko et al. 2002) and (Langner et al. 2003)

in this analysis, the Continuous Wavelet Transform (CWT) was used which represents a wave in two dimensions: data number and wavelength.

CWT is given:

$$CWT(u, s) = \int_{-\infty}^{\infty} h(t) \frac{1}{|s|^{0.5}} \Psi^* \left(\frac{t-u}{s} \right) dt \quad (32)$$

Where s is the scale, u is the displacement, Ψ is the mother wavelet, and $*$ means complex conjugate and t is the coordinate in time (Cooper & Cowan 2008) Equation 32 can also be expressed in spatial terms (Teolis 2017):

$$\Psi(x) = \frac{1}{\pi f_b} e^{2\pi i f_c x} e^{-\frac{x^2}{f_b}} \quad (33)$$

The conventional semblance is a normalized coherence measure, first computed in 1969 (Taner & Koehler 1969), later, Neidell and Taner (Neidell & Taner 1971) found that the coherence and semblance were two different operators. Thus, semblance was expressed as shown in the equation 34:

$$S_{NT} [i] = \frac{\sum_{j=i-M}^{i+M} \left(\sum_{k=0}^{N-1} q[j, k] \right)^2}{N \sum_{j=i-M}^{i+M} \sum_{k=0}^{N-1} q[j, k]^2} \quad (34)$$

Where i, j are time sample indices, k is a trace number, $q[j, k]$ is the trace amplitude at time index j a trace number k of the NMO-corrected gather.

To reduce and smooth the decays a boxcar filter is often applied, that can be written as (Luo et al. 2015):

$$S_C [i] = \frac{\sum_j h[i-j] \left(\sum_k q[j, k] \right)^2}{N \sum_j h[i-j] \sum_k q[j, k]^2} \quad (35)$$

There is an alternative expression for the conventional semblance, which can be expressed as a normalized correlation coefficient. However, first, a trace $r[j]$ should be defined as a summation over the trace number:

$$r[j] \equiv \sum_k q[j, k] \quad (36)$$

Therefore:

$$C_{rq} [i] \equiv \sum_j h[i-j] \sum_k r[j] q[j, k] \quad (37)$$

$$C_{rr} [i] \equiv \sum_j h[i-j] \sum_k r[j]^2 \quad (38)$$

$$C_{qq} [i] \equiv \sum_j h[i-j] \sum_k q[j, k]^2 \quad (39)$$

Now, the three equations 37, 38 and 39 can be expressed as a conventional semblance (Luo et al. 2015):

$$S_C [i] = \frac{C_{rq} [i]^2}{C_{rr} [i] C_{qq} [i]} \quad (40)$$

7. COUNT RATES FROM GROUND-BASED DETECTORS

The neutrons detected at ground level are the product of atmospheric showers caused by the collision of primary particles with molecules in the atmosphere. The neutron count is given by the following equation:

$$N(P_c, x, t) = \int_{P_c}^{\infty} \left(\frac{-dN}{dP} \right) dP = \sum_i \int_{P_c}^{\infty} S_i(P, x) j_i(P, t) dP \quad (41)$$

Where $j_i(P, t)$ is the spectrum of the primary species above the atmosphere, and $S_i(P, x)$ is the atmospheric yield function due to this species. P_c is the cut-off rigidity, which is the necessary minimum energy for a particle to enter the Earth's magnetosphere. The quantity $dN = dP$ is the differential counting rate of the instrument inside the atmosphere. The yield function used in this analysis is the following (Caballero-Lopez & Moraal 2012):

$$S_H = \frac{-(dN/dP)}{J_H(P) + 1.584F(P)j_{He}} \quad (42)$$

where $F(P)$ is the ratio between the yield functions of H_e and H as reported by (Clem & Dorman 2000):

$$F(P) = F_0(P_0^a + P^a)^{(\gamma_1 - \gamma_2/a)} P \gamma^2 \quad (43)$$

the values in the equation are: $F_0 = 2.0$, $\gamma_1 = 0$, $\gamma_2 = 10$, $a = 1.4$ and $P_0 = 0.45$.

The equation 42 allows computing a modulation factor and will be used to obtain the semblance. The J_H and J_{He} terms in the equation 42 are the transport equation solutions (convection-diffusion or force field), which are in terms of a LIS previously mentioned. A Python code has been programmed and can be found at <https://github.com/JorUrie/TRC.git>

8. FIRST ANALYSIS

The first analysis consists of three stations located in different magnetospheric latitudes (Table 2) and computing their modulation factor, then semblance between the modulation factor and sunspots or mean solar magnetic field will be computed. The data were downloaded from the Neutron Monitor DataBase (NMDB)², sunspot data from Sunspot

² NMDB

Number³ (Figure 3) and mean solar magnetic field data from The Wilcox Solar Observatory⁴ (Figure 4).

Neutron Monitor	Cut-off Rigidity [GeV]
Antarctic (SNAE)	0.73
Finland (OULU)	0.81
Kazakhstan (AATB)	5.90

Table 2: Cut-off Rigidity from the stations used in the first analysis

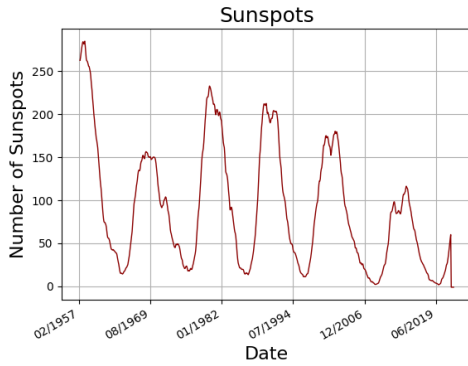


Figure 3: Sunspots data obtained from Sunspot index and Long-term Solar Observations.

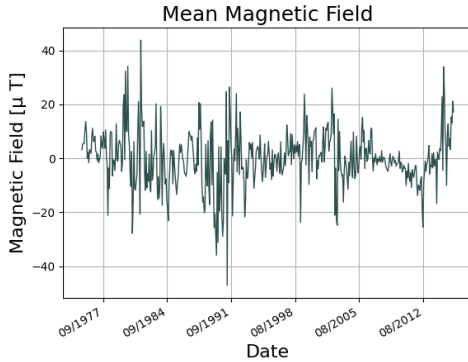


Figure 4: Solar Magnetic Field date obtained from The Wilcox Solar Observatory.

The Figure 3 shows the number of sunspots recorded, which are related to solar maximums and minimums. The data covers from May 1957 to July 2022. In the same figure, solar cycles can be observed, in other words, solar maximums belong approximately to the years 1958, 1970, 1980, 1990, 2014 and the next solar maximum could be in 2024. Solar minimums belong approximately to the years 1965, 1976,

³ Sunspot Number | SILSO (sidc.be)

⁴ WSO -The Wilcox Solar Observatory (stanford.edu)

1986, 1997 and 2010. With the previous information, 11-year cycle can be perceived. In 1958 was the largest recorded maximum, while the smallest maximum was in 1970. Conversely, minimums have similar values and there are not many differences.

The mean magnetic field information belongs to the dates from May 1975 to December 2015. The information has cusps and appears not to have significant changes, but in September 1981 was the biggest registered maximum, while in March 1991 was the smallest registered value. If a line is traced along the graphic following a “regression”, maximums and minimums can be identified, they would be mostly inversely proportionate to sunspots.

The selected stations were SNAE (south), OULU (north) and AATB (magnetic equator). They were deemed appropriate based on their respective latitudes in the Earth (Figure 24). SNAE, OULU and AATB data are shown in the figures 5, 6 and 7. The data were downloaded and normalized to the highest contained value.

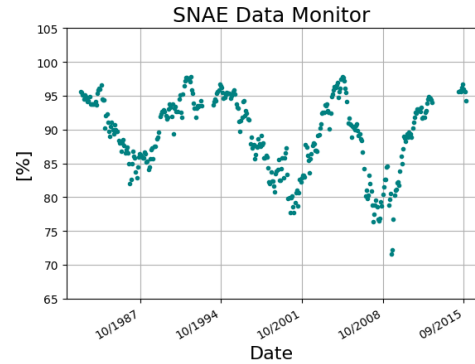


Figure 5: SNAE data obtained from NMDB.

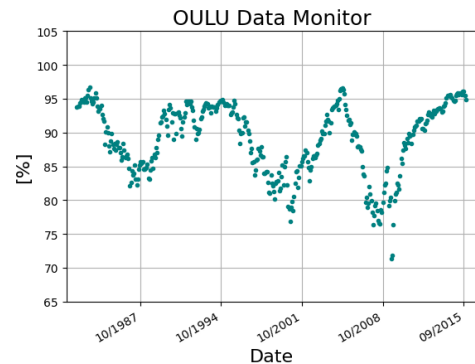


Figure 6: OULU data obtained from NMDB.

The previously mentioned Figures 5, 6 and 7 are normalized data, because the data is obtained from the neutron monitors on the Earth. However, the particles have already been modified by modulation phenomena and they have also lost energy (secondary cosmic rays), for that reason a modulation factor is necessary to compute.

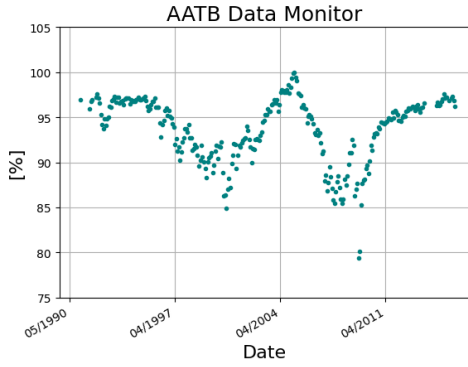


Figure 7: AATB data obtained from NMDB.

Non-normalized data have been introduced into the atmospheric yield function, which requires both a LIS and a transport equation solution (convection-diffusion or force field) to compute the modulation factor.

The figures from 8 to 15 are the modulation factors for the same station using every previously mentioned LIS and a transport equation solution. Their unities are *Counts/s* and *Date*, because the modulation factor is the amount of particles before they enter the Earth's atmosphere and interact with the particles in a given date. Modulation factor would not be necessary if the satellites would take desired measurements, but the technology and the conditions do not allow it.

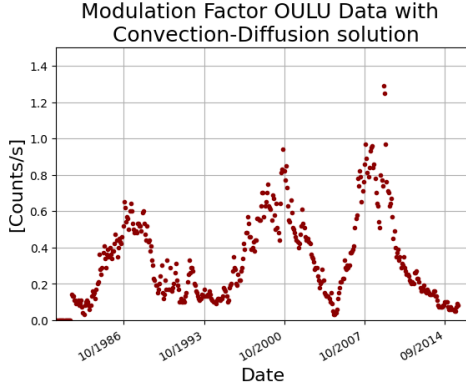


Figure 8: OULU station. Modulation factor with Convection-Diffusion solution using Lagner, Potgieter and Webber LIS in 2003.

The modulation factors were computed for all selected stations. Those have a similar pattern for each LIS and are also similar to the downloaded data, for example, in Figures 6 and 8, high values can be observed, in 1987 near to 2004 and 2011. These patterns also occur in Figures 8 to 15. In fact, in Figures 8, 10, 12 and 14 between values 1.2 and 1.4 *Counts/s*, two points are always present and are also the highest values. For the figures 9, 11, 13 and 15, the same pattern is observed and the two highest points are also present between 1.5 and 1.75 *Counts/s*. The main difference among

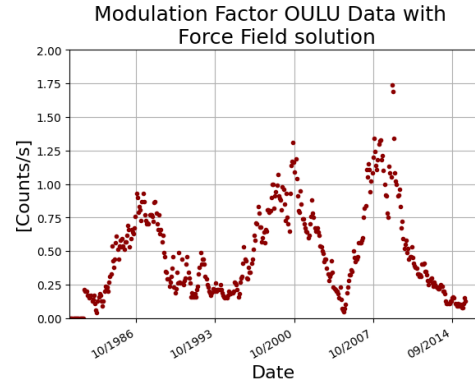


Figure 9: OULU station. Modulation factor with Force Field solution using Lagner, Potgieter and Webber LIS in 2003.

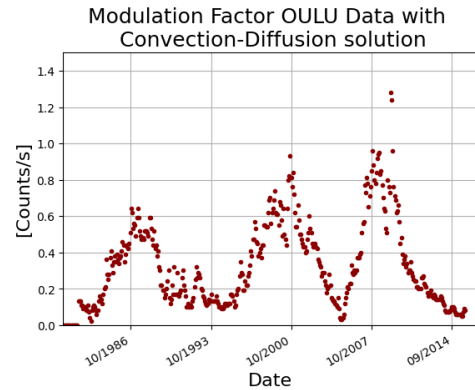


Figure 10: OULU station. Modulation factor with Convection-Diffusion solution using Burguer and Potgieter LIS in 2000.

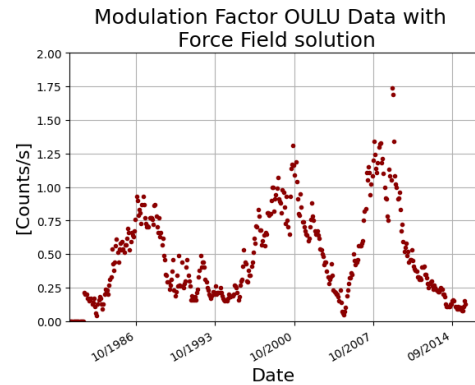


Figure 11: OULU station. Modulation factor with Force Field solution using Burguer and Potgieter LIS in 2000.

modulation factors using convection-diffusion and force field solutions is the amplitude.

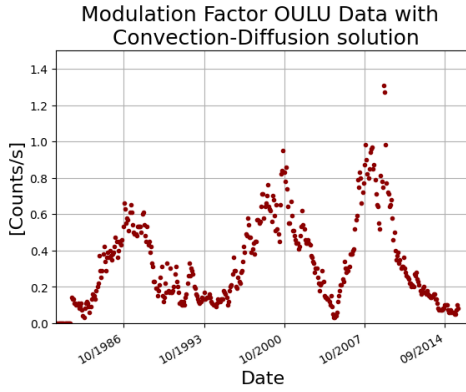


Figure 12: OULU station. Modulation factor with Convection-Diffusion solution using Garcia-Munoz, Mason and Simpson LIS in 1975.

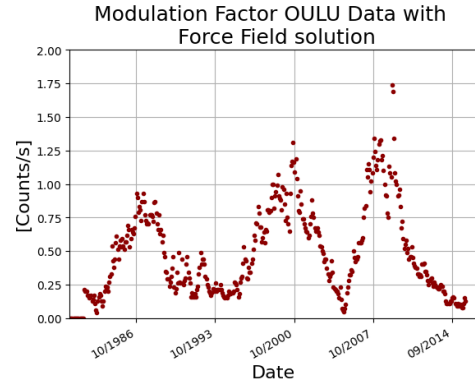


Figure 15: OULU station. Modulation factor with Force Field solution using Ghelfi, Barao, Derome and Maurin LIS in 2017.

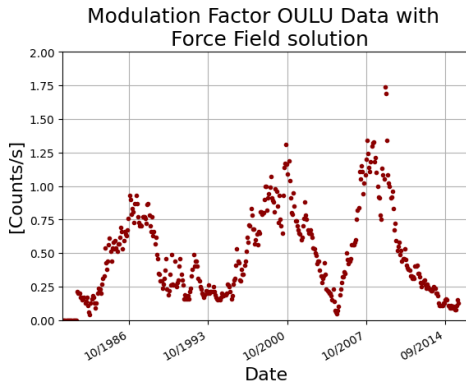


Figure 13: OULU station. Modulation factor with Force Field solution using Garcia-Munoz, Mason and Simpson LIS in 1975.

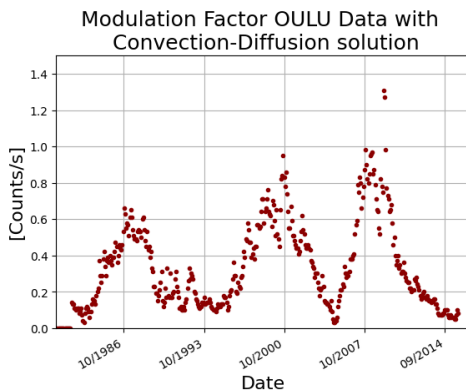


Figure 14: OULU station. Modulation factor with Convection-Diffusion solution using Ghelfi, Barao, Derome and Maurin LIS in 2017.

From Figures 8 to 15 also looks like the figure 3, because more extragalactic cosmic rays are introduced into the Earth as a result of low solar modulation.

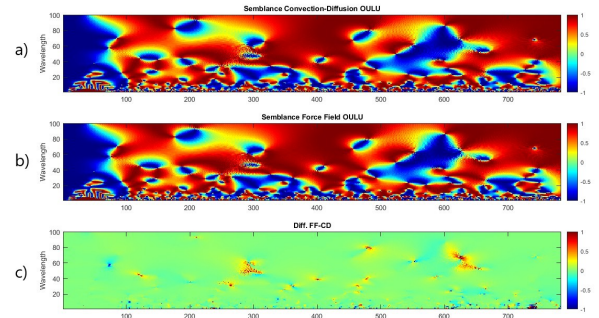


Figure 16: OULU Station a) Semblance between Modulation Factor using Convection-Diffusion with Lagner, Potgieter and Webber LIS in 2003 vs Sunspot data. b) Semblance between Modulation Factor using Force Field with Lagner, Potgieter and Webber LIS in 2003 vs Sunspot data. c) Difference between the two previous semblances.

For the three stations selected according to their latitude, the semblance for the modulation factor and sunspots using several LIS are shown. However, only the results for the OULU station are presented here; the remaining models can be found in the appendix.

The computed models offer similar results among them (figures a) and b) for each semblance figure). They even appear as if they were the same model, but thanks to the difference between semblances (figures c)) it is possible to observe small differences, mainly in Figures 21 and 20. If both figures previously mentioned are compared with the rest of the respective semblances in this section, the main difference is in the interval 50 to 100 in number of data and 40 to 80 in the wavelength, where a blue spot changes its size and shape.

There is correlation between sunspots and modulation phenomena, which can be observed in the figures 16, 18, 20 and 22 highlighted in red. There is anti-correlation between

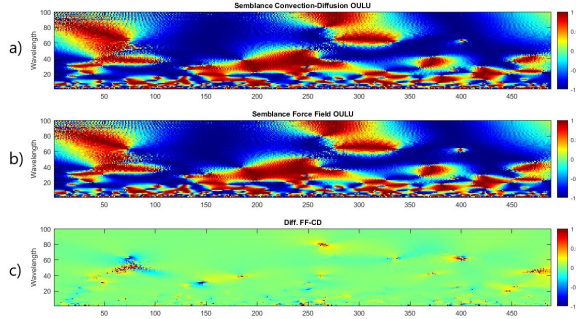


Figure 17: OULU Station a) Semblance between Modulation Factor using Convection-Diffusion with Lagner, Potgieter and Webber LIS in 2003 vs Mean Magnetic Field data. b) Semblance between Modulation Factor using Mean Magnetic Field with Lagner, Potgieter and Webber LIS in 2003 vs Sunspot data. c) Difference between the two previous semblances.

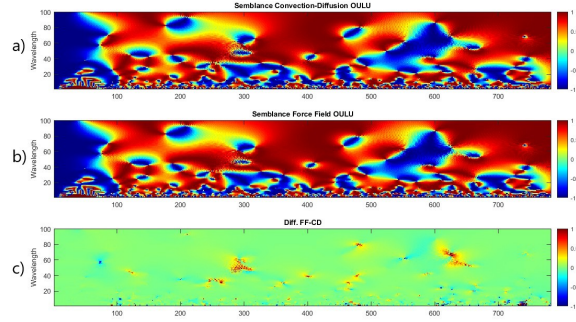


Figure 18: OULU Station a) Semblance between Modulation Factor using Convection-Diffusion with Burguer and Potgieter LIS in 2000 vs Sunspot data. b) Semblance between Modulation Factor using Force Field with Burguer and Potgieter LIS in 2000 vs Sunspot data. c) Difference between the two previous semblances.

the mean solar magnetic field and the modulation phenomena observed in blue. Both behaviors are maintained independently of the magnetospheric latitude.

9. SECOND ANALYSIS

The same calculations were performed, but the modulation factors were averaged. The data used for the following analysis were: KERG, MOSC, OULU, THUL, and HRMS (Table 3). This analysis was conducted to generalize the previous results and to analyze which LIS have the best fit.

The Figure 24 are the position of the used stations in both analyses.

The Figures 25 to 32 are the modulation factors averaged using convection-diffusion and force field solutions with Lagner, Potgieter & Webber LIS in 2003, Burguer & Potgi-

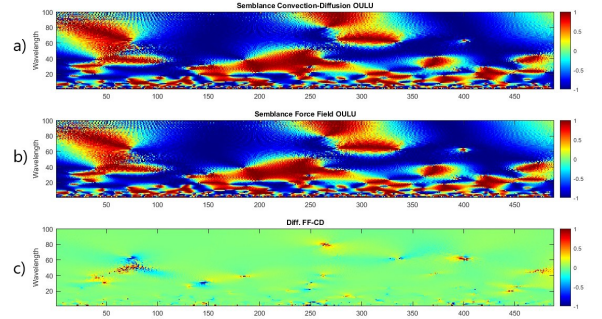


Figure 19: OULU Station a) Semblance between Modulation Factor using Convection-Diffusion with Burguer and Potgieter LIS in 2000 vs Mean Magnetic Field data. b) Semblance between Modulation Factor using Force Field with Burguer and Potgieter LIS in 2000 vs Mean Magnetic Field data. c) Difference between the two previous semblances.

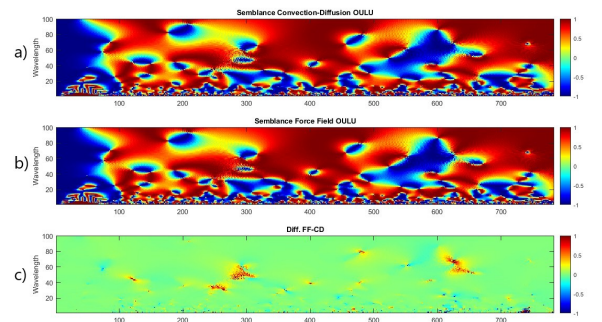


Figure 20: OULU Station a) Semblance between Modulation Factor using Convection-Diffusion with Garcia-Munoz, Mason and Simpson LIS in 1975 vs Sunspot data. b) Semblance between Modulation Factor using Force Field with Garcia-Munoz, Mason and Simpson LIS in 1975 vs Sunspot data. c) Difference between the two previous semblances.

Neutron Monitor	Cut-off Rigidity [GeV]
Greenland (THUL)	0.3
Finland (OULU)	0.81
Kerguelen (KERG)	1.14
Moscow (MOSC)	2.43
Hermanus (HRMS)	4.58

Table 3: Cut-off Rigidity from the used stations in the second analysis

eter LIS in 2000, Garcia-Munoz, Mason & Simpson LIS in 1975 and Ghelfi, Barao, Derome & Maurin LIS in 2017.

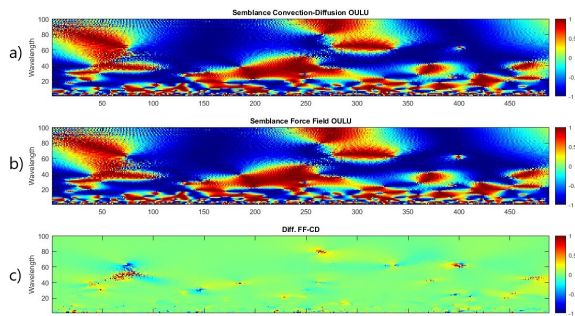


Figure 21: OULU Station a) Semblance between Modulation Factor using Convection-Diffusion with Garcia-Munoz, Mason and Simpson LIS in 1975 vs Mean Magnetic Field data. b) Semblance between Modulation Factor using Force Field with Garcia-Munoz, Mason and Simpson LIS in 1975 vs Mean Magnetic Field data. c) Difference between the two previous semblances.

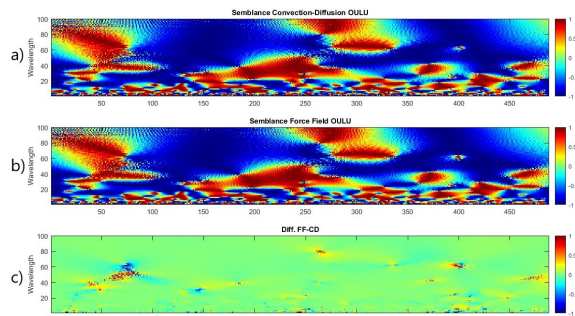


Figure 23: OULU Station a) Semblance between Modulation Factor using Convection-Diffusion with Ghelfi, Barao, Derome and Maurin LIS in 2017 vs Mean Magnetic Field data. b) Semblance between Modulation Factor using Force Field with Ghelfi, Barao, Derome and Maurin LIS in 2017 vs Mean Magnetic Field data. c) Difference between the two previous semblances.

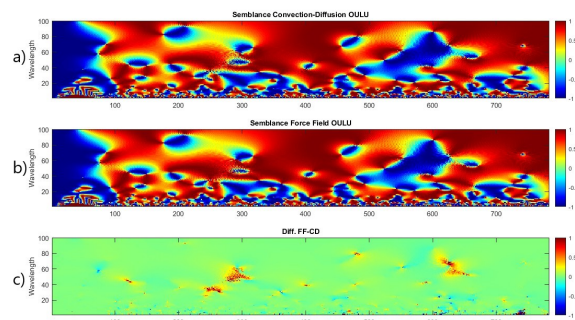


Figure 22: OULU Station a) Semblance between Modulation Factor using Convection-Diffusion with Ghelfi, Barao, Derome and Maurin LIS in 2017 vs Sunspots data. b) Semblance between Modulation Factor using Force Field with Ghelfi, Barao, Derome and Maurin LIS in 2017 vs Sunspots data. c) Difference between the two previous semblances.

The Figures 33 to 48 show the semblance between the aforementioned modulation factors with sunspots and mean magnetic field data. The figures 34, 36, 38, 40 and 42 show the percentage of zeros contained in the difference between semblance (Figures c)). Thanks to this analysis, the LIS models were selected because they offer the most reliable results.

In this case, an average modulation factor of several neutron detectors around the world was computed to analyze the general analyze between sunspots and mean solar magnetic field and modulation phenomena. The results were utterly similar to the first analysis, in fact the analysis of the contained zeros confirms the hypothesis, that there is a correlation between sunspots and modulation phenomena and an anti-correlation between the mean magnetic field and mod-

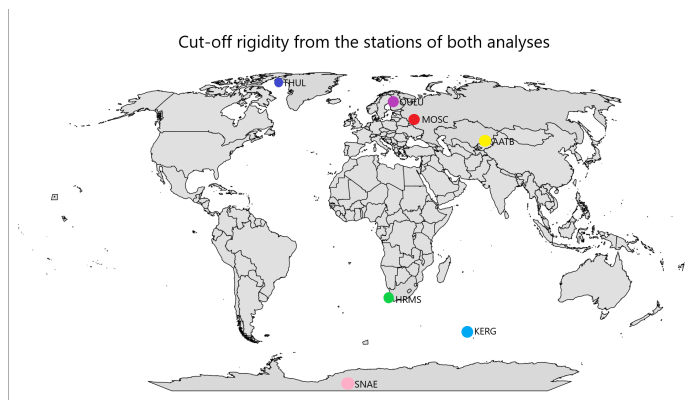


Figure 24: Position of the neutron monitors around the world used in both analyses

ulation phenomena. The analysis of the zeros is summarized in Table 4.

Analysis of contained zeros	Sunspots		Mean Magnetic Field	
	<0	>0	<0	> 0
Webber & Lockwood	47	53	46	54
Burguer	47	53	46	54
Garcia-Munoz	49	51	47	53
Maurin	49	51	46	54

Table 4: Analysis of contained zeros from difference between semblance using transport equation solution convection-diffusion and force field and different LIS

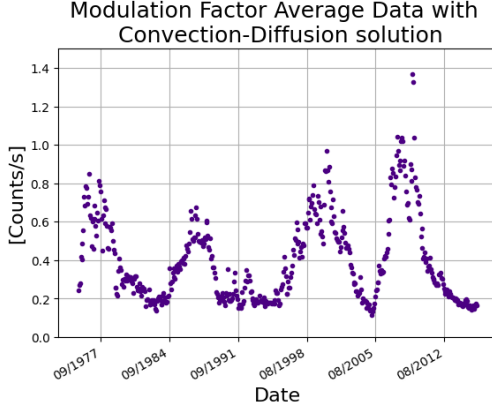


Figure 25: Averaged Modulation Factor among KERG, HRMS, MOSC, OULU and THUL stations. Modulation factor with Convection-Diffusion solution using Lagner, Potgieter & Webber LIS in 2003.

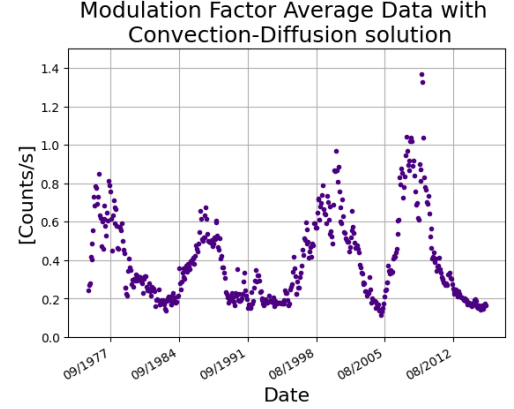


Figure 27: Averaged Modulation Factor among KERG, HRMS, MOSC, OULU and THUL stations. Modulation factor with Convection-Diffusion solution using Burguer and Potgieter LIS in 2000.

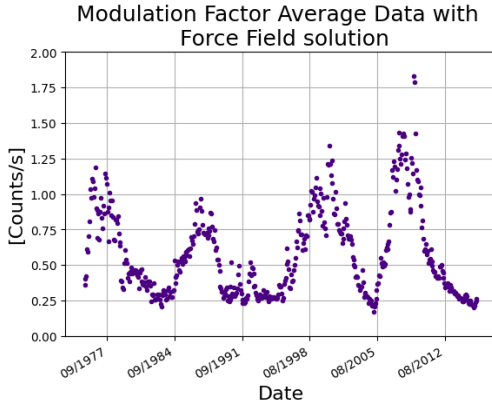


Figure 26: Averaged Modulation Factor among KERG, HRMS, MOSC, OULU and THUL stations. Modulation factor with Force Field solution using Lagner, Potgieter & Webber LIS in 2003..

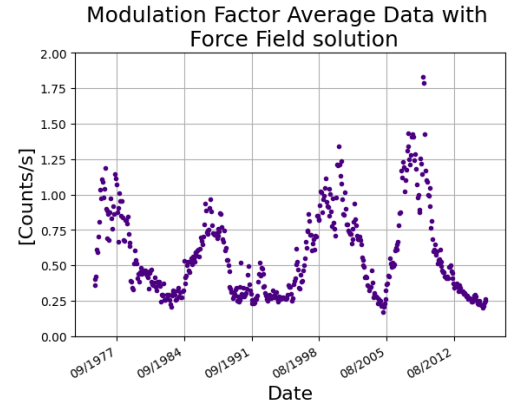


Figure 28: Averaged Modulation Factor among KERG, HRMS, MOSC, OULU and THUL stations. Modulation factor with Force Field solution using Burguer and Potgieter LIS in 2000.

10. CONCLUSIONS

Both analyses allow quantifying the correlation between the modulation factor and sunspots and anti-correlation between the modulation factor and the mean magnetic field. The models are mostly similar with both transport equation solutions and the local interstellar spectrum as they only show slight changes.

For the first analysis, the the modulation factor yields similar outcomes and are solely dependent on the rigidity factor. The correlation between sunspots and modulation factor is more pronounced for stations closer to the magnetic poles, such as OULU and SNAE, than for the equatorial AATB station. However, this pattern is not replicated for the semblance between the modulation factor and the mean

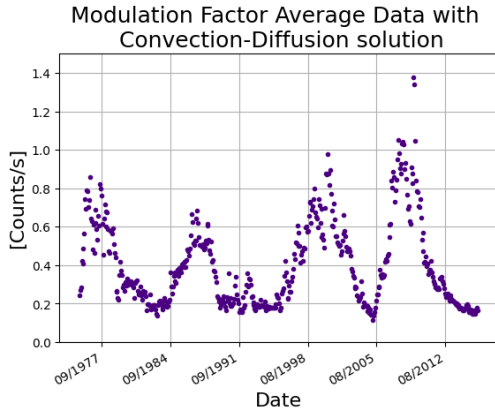


Figure 29: Averaged Modulation Factor among KERG, HRMS, MOSC, OULU and THUL stations. Modulation factor with Convection-Diffusion solution using Garcia-Munoz, Mason and Simpson LIS in 1975.

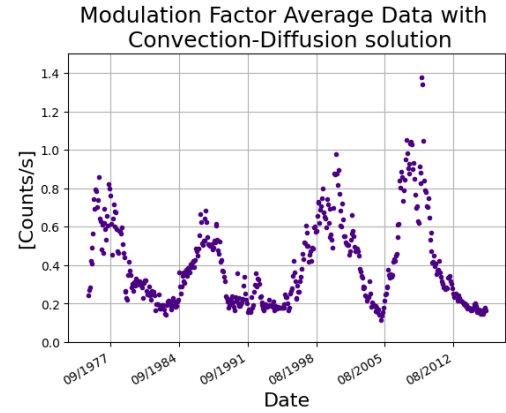


Figure 31: Averaged Modulation Factor among KERG, HRMS, MOSC, OULU and THUL stations. Modulation factor with Convection-Diffusion solution using Ghelfi, Barao, Derome and Maurin LIS in 2017.

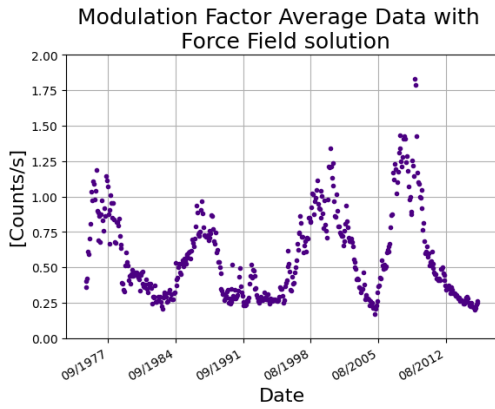


Figure 30: Averaged Modulation Factor among KERG, HRMS, MOSC, OULU and THUL stations. Modulation factor with Force Field solution using Garcia-Munoz, Mason and Simpson LIS in 1975.

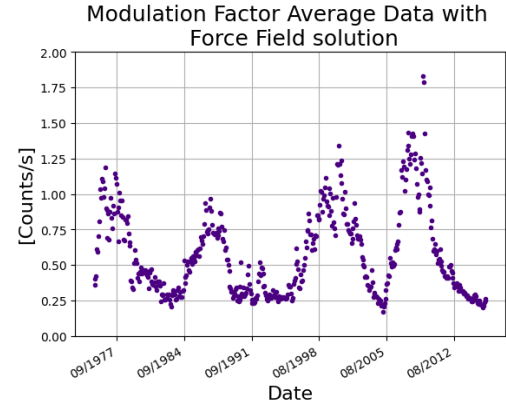


Figure 32: Averaged Modulation Factor among KERG, HRMS, MOSC, OULU and THUL stations. Modulation factor with Force Field solution using Ghelfi, Barao, Derome and Maurin LIS in 2017.

magnetic field. The station near the magnetic equator has shows more anti-correlation than near the poles. The pattern is similar for every semblance, even when different LIS and transport equation solutions were used.

Thanks to the second analysis, the first analysis can be affirmed and generalized, the force field solution is also more compatible with neutron detectors data. Additionally, any modulation factor solution will be similar to the neutron detector data and will only have minimal amplitude variations.

In the second analysis, it is possible to observe similarity among the graphs of contained zeros in the difference of semblances, particularly when the modulation factors have been computed by different LIS. However, if semblance is computed using the Garcia-Munoz, Mason and Simpson LIS in 1975 more differences are observed. These differences are visible in the analysis of contained zeros for semblance between averaged modulation factor and mean magnetic field.

According to the table 4 semblance using sunspots and averaged modulation factors data is very similar, and the percentage of contained zeros is comparable when using the Webber & Lockwood and Burguer and Potgieter LIS in 2000 or Garcia-Munoz and Ghelfi, Barao, Derome and Maurin LIS in 2017 are used.

Therefore, the LIS, that have the best adjust to the semblance model are Lagner, Potgieter and Webber LIS in 2003, Burguer and Ghelfi, Barao, Derome and Maurin LIS in 2017 using force field solution as they offer more consistent values, as shown in Table 4.

With both proposed models, it can be asserted that there is a correlation between modulation phenomena and sunspots, because the solar activity is less allowed to detect more rays from the Sun. The anti-correlation between modulation phenomena and the mean magnetic field is due to high solar activity. Therefore, fewer solar rays affect the arrival of cosmic rays from other sources.

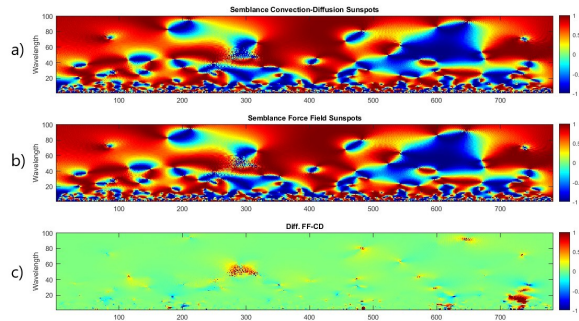


Figure 33: Average among HRMS, KERG, MOSC, OULU and THUL a) Semblance between Average Modulation Factor using Convection-Diffusion with Lagner, Potgieter and Webber LIS in 2003 vs Sunspots data. b) Semblance between Average Modulation Factor using Force Field with Lagner, Potgieter and Webber LIS in 2003 vs Sunspots data. c) Difference between the two previous semblances.

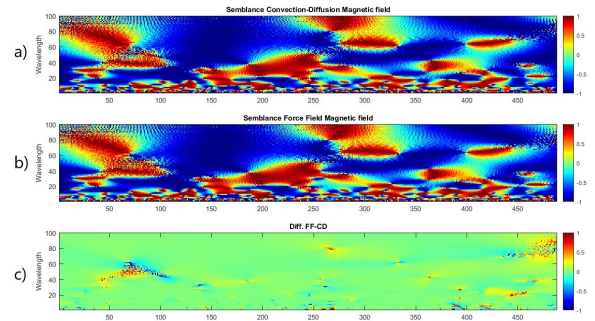


Figure 35: Average among HRMS, KERG, MOSC, OULU and THUL a) Semblance between Average Modulation Factor using Convection-Diffusion with Lagner, Potgieter and Webber LIS in 2003 vs Solar Magnetic Field data. b) Semblance between Average Modulation Factor using Force Field with Lagner, Potgieter and Webber LIS in 2003 vs Solar Magnetic Field data. c) Difference between the two previous semblances.

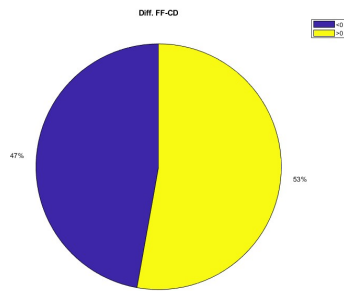


Figure 34: Contained zeros into Figure 33 c).

Thanks to this proposed quantitative model, a more precise predictive model of cosmic rays with solar activity can be computed.

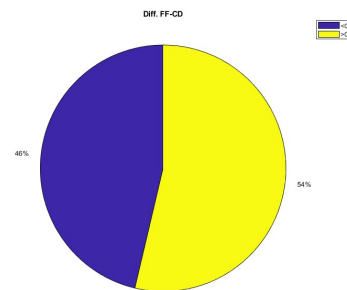


Figure 36: Contained zeros into Figure 35 c).

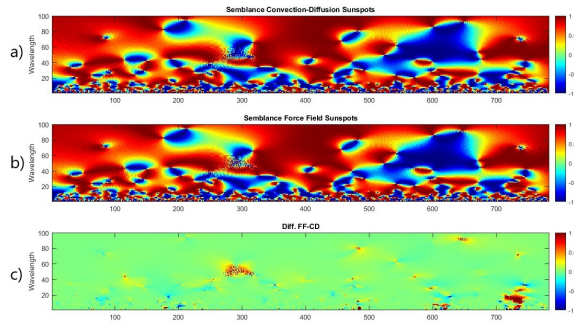


Figure 37: Average among HRMS, KERG, MOSC, OULU and THUL a) Semblance between Average Modulation Factor using Convection-Diffusion with Burguer and Potgieter LIS in 2000 vs Sunspots data. b) Semblance between Average Modulation Factor using Force Field with Burguer and Potgieter LIS in 2000 vs Sunspots data. c) Difference between the two previous semblances.

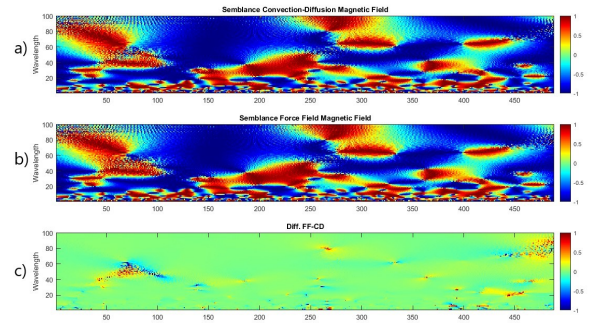


Figure 39: Average among HRMS, KERG, MOSC, OULU and THUL a) Semblance between Average Modulation Factor using Convection-Diffusion with Burguer and Potgieter LIS in 2000 vs Solar Magnetic Field data. b) Semblance between Average Modulation Factor using Force Field with Burguer and Potgieter LIS in 2000 vs Solar Magnetic Field data. c) Difference between the two previous semblances.

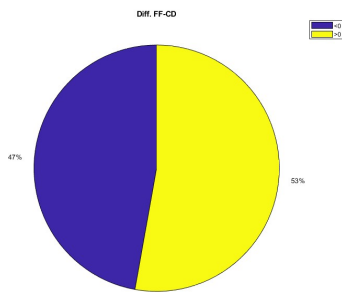


Figure 38: Contained zeros into Figure 37 c).

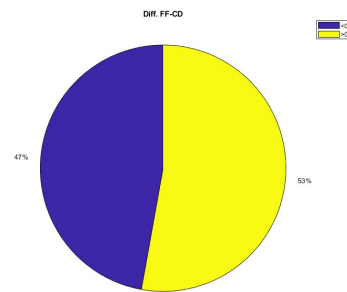


Figure 40: Contained zeros into Figure 39 c).

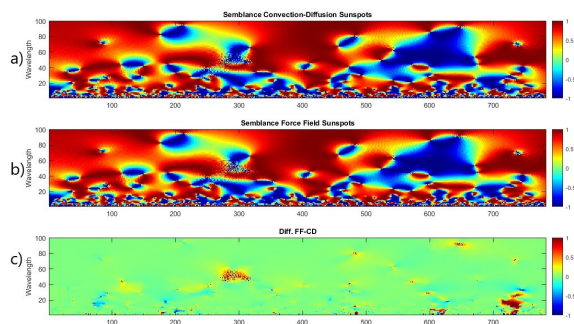


Figure 41: Average among HRMS, KERG, MOSC, OULU and THUL a) Semblance between Average Modulation Factor using Convection-Diffusion with Garcia-Munoz, Mason and Simpson LIS in 1975 vs Sunspots data. b) Semblance between Average Modulation Factor using Force Field with Garcia-Munoz, Mason and Simpson LIS in 1975 vs Sunspots data. c) Difference between the two previous semblances.

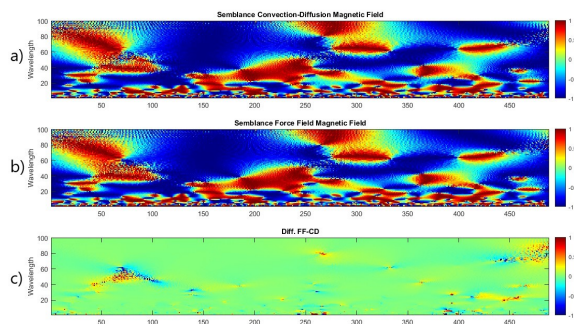


Figure 43: Average among HRMS, KERG, MOSC, OULU and THUL a) Semblance between Average Modulation Factor using Convection-Diffusion with Garcia-Munoz, Mason and Simpson LIS in 1975 vs Solar Magnetic Field data. b) Semblance between Average Modulation Factor using Force Field with Garcia-Munoz, Mason and Simpson LIS in 1975 vs Solar Magnetic Field data. c) Difference between the two previous semblances.

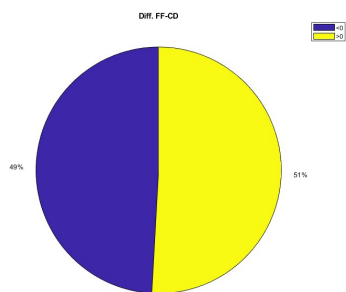


Figure 42: Contained zeros into Figure 41 c).

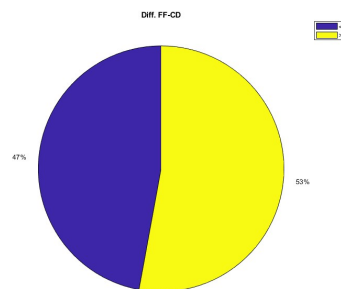


Figure 44: Contained zeros into Figure 43 c).

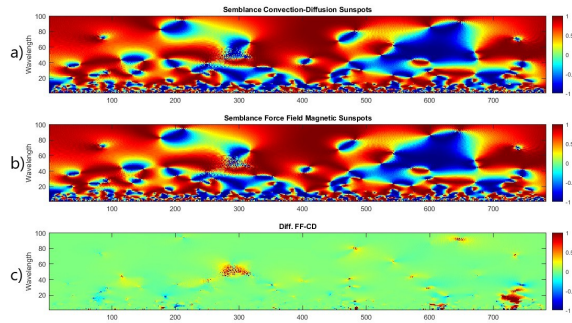


Figure 45: Average among HRMS, KERG, MOSC, OULU and THUL a) Semblance between Average Modulation Factor using Convection-Diffusion with Ghelfi, Barao, Derome and Maurin LIS in 2017 vs Sunspots data. b) Semblance between Average Modulation Factor using Force Field with Ghelfi, Barao, Derome and Maurin LIS in 2017 vs Sunspots data. c) Difference between the two previous semblances.

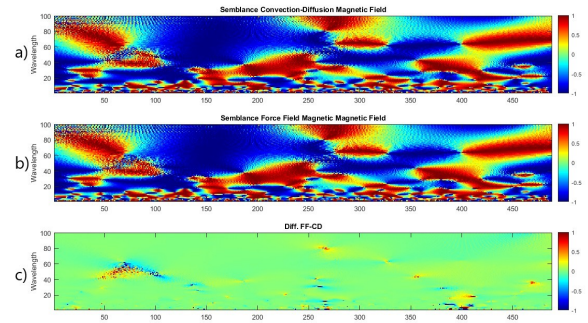


Figure 47: Average among HRMS, KERG, MOSC, OULU and THUL a) Semblance between Average Modulation Factor using Convection-Diffusion with Ghelfi, Barao, Derome and Maurin LIS in 2017 vs Solar Magnetic Field data. b) Semblance between Average Modulation Factor using Force Field with Ghelfi, Barao, Derome and Maurin LIS in 2017 vs Solar Magnetic Field data. c) Difference between the two previous semblances.

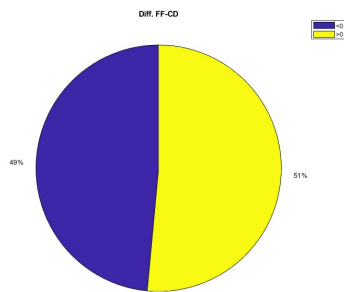


Figure 46: Contained zeros into Figure 45 c).

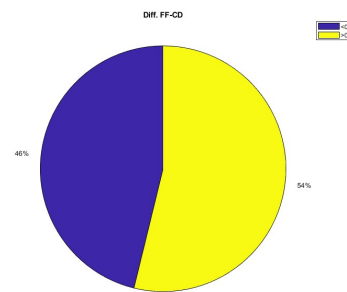


Figure 48: Contained zeros into Figure 47 c).

REFERENCES

- Auger, P., Ehrenfest, P., Maze, R., Daudin, J., & Fréon, R. A. 1939, *Reviews of Modern Physics*, 11, 288, doi: [10.1103/RevModPhys.11.288](https://doi.org/10.1103/RevModPhys.11.288)
- Bieber, J. 1999, in *International Cosmic Ray Conference*, Vol. 7, 26th International Cosmic Ray Conference (ICRC26), Volume 7, 61
- Boschini, M. J., Della Torre, S., Gervasi, M., et al. 2017, *ApJ*, 840, 115, doi: [10.3847/1538-4357/aa6e4f](https://doi.org/10.3847/1538-4357/aa6e4f)
- Burger, R. A., Potgieter, M. S., & Heber, B. 2000, *Journal of Geophysical Research: Space Physics*, 105, 27447, doi: <https://doi.org/10.1029/2000JA000153>
- Caballero-Lopez, R. A., & Moraal, H. 2004, *Journal of Geophysical Research: Space Physics*, 109, doi: <https://doi.org/10.1029/2003JA010098>
- . 2012, *Journal of Geophysical Research: Space Physics*, 117, doi: <https://doi.org/10.1029/2012JA017794>
- Clem, J., & Dorman, L. 2000, *Space Science Reviews*, 93, doi: [10.1023/A:1026508915269](https://doi.org/10.1023/A:1026508915269)
- Cooper, G. R. J., & Cowan, D. R. 2008, *Computers and Geosciences*, 34, 95, doi: [10.1016/j.cageo.2007.03.009](https://doi.org/10.1016/j.cageo.2007.03.009)
- Crank, J., & Nicolson, P. 1947, *Mathematical Proceedings of the Cambridge Philosophical Society*, 43, 50–67, doi: [10.1017/S0305004100023197](https://doi.org/10.1017/S0305004100023197)
- Ferrari, A., Ranft, J., Roesler, S., & Sala, P. R. 1996, *Zeitschrift für Physik C: Particles and Fields*, 71, 75, doi: [10.1007/s002880050149](https://doi.org/10.1007/s002880050149)
- Fisk, L. A., Goldstein, M. L., Klimas, A. J., & Sandri, G. 1974, *ApJ*, 190, 417, doi: [10.1086/152893](https://doi.org/10.1086/152893)
- Garcia-Munoz, M., Mason, G. M., & Simpson, J. A. 1975, *ApJ*, 202, 265, doi: [10.1086/153973](https://doi.org/10.1086/153973)
- Ghelfi, A., Barao, F., Derome, L., & Maurin, D. 2017, *Astronomy & Astrophysics*, 605, C2, doi: [10.1051/0004-6361/201527852e](https://doi.org/10.1051/0004-6361/201527852e)
- Gleeson, L. J., & Axford, W. I. 1968, *Canadian Journal of Physics Supplement*, 46, 937, doi: [10.1139/p68-388](https://doi.org/10.1139/p68-388)
- James, F. a. 1998. <https://cds.cern.ch/record/2296388>
- Langner, U. W., Potgieter, M. S., & Webber, W. R. 2003, *Journal of Geophysical Research: Space Physics*, 108, doi: <https://doi.org/10.1029/2003JA009934>
- Luo, X., Zhang, M., Potgieter, M., Feng, X., & Pogorelov, N. V. 2015, *ApJ*, 808, 82, doi: [10.1088/0004-637X/808/1/82](https://doi.org/10.1088/0004-637X/808/1/82)
- Moskalenko, I. V., Strong, A. W., Ormes, J. F., & Potgieter, M. S. 2002, *The Astrophysical Journal*, 565, 280, doi: [10.1086/324402](https://doi.org/10.1086/324402)
- Neidell, N. S., & Taner, M. T. 1971, *GEOPHYSICS*, 36, 482, doi: [10.1190/1.1440186](https://doi.org/10.1190/1.1440186)
- O'Neill, P. M. 2006, *Advances in Space Research*, 37, 1727, doi: [10.1016/j.asr.2005.02.001](https://doi.org/10.1016/j.asr.2005.02.001)
- Parker, E. N. 1965, *Planet. Space Sci.*, 13, 9, doi: [10.1016/0032-0633\(65\)90131-5](https://doi.org/10.1016/0032-0633(65)90131-5)
- Potgieter, M., De Simone, N., Vos, E., Boezio, M., & Di Felice, V. 2012, in *39th COSPAR Scientific Assembly*, Vol. 39, 1526
- Putze, A., & Derome, L. 2014, *Physics of the Dark Universe*, 5, 29, doi: [10.1016/j.dark.2014.07.002](https://doi.org/10.1016/j.dark.2014.07.002)
- Sartini, L., Simeone, F., Pani, P., et al. 2010, *Nuclear Instruments and Methods in Physics Research A*
- Sekido, Y., & Elliot, H. 1985, *Early history of cosmic ray studies: Personal reminiscences with old photographs.* <https://www.osti.gov/biblio/7169147>
- Shikaze, Y., Haino, S., Abe, K., et al. 2007, *Astroparticle Physics*, 28, 154, doi: [10.1016/j.astropartphys.2007.05.001](https://doi.org/10.1016/j.astropartphys.2007.05.001)
- Strong, A. W., Moskalenko, I. V., & Ptuskin, V. S. 2007, *Annual Review of Nuclear and Particle Science*, 57, 285, doi: [10.1146/annurev.nucl.57.090506.123011](https://doi.org/10.1146/annurev.nucl.57.090506.123011)
- Tan, L. C., & Ng, L. K. 1983, *ApJ*, 269, 751, doi: [10.1086/161084](https://doi.org/10.1086/161084)
- Taner, M. T., & Koehler, F. 1969, *GEOPHYSICS*, 34, 859, doi: [10.1190/1.1440058](https://doi.org/10.1190/1.1440058)
- Teolis, A. 2017, *Computational Signal Processing with Wavelets*, doi: [10.1007/978-3-319-65747-9](https://doi.org/10.1007/978-3-319-65747-9)
- Vos, E. E., & Potgieter, M. S. 2015, *ApJ*, 815, 119, doi: [10.1088/0004-637X/815/2/119](https://doi.org/10.1088/0004-637X/815/2/119)

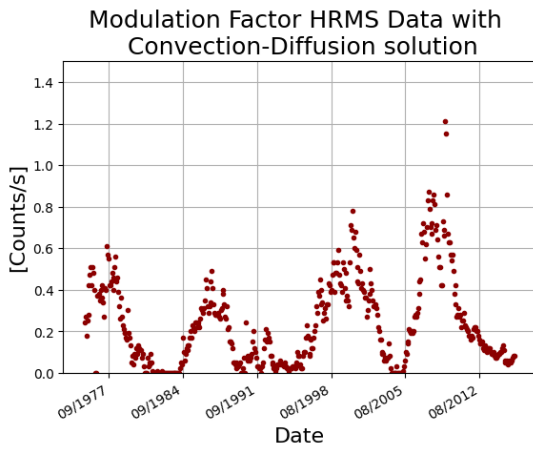


Figure 49: HRMS station. Modulation factor with Convection-Diffusion using Lagner, Potgieter & Webber LIS in 2003

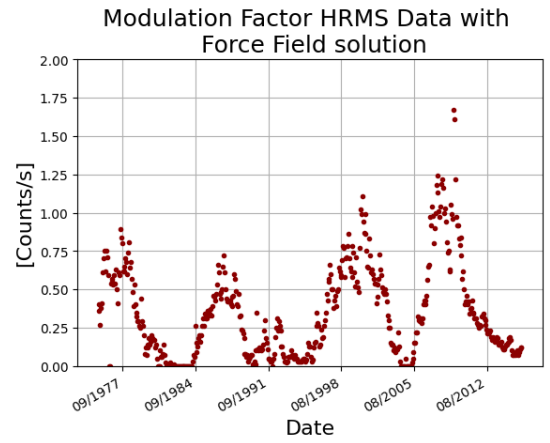


Figure 50: HRMS station. Modulation factor with Force Field using Lagner, Potgieter & Webber LIS in 2003

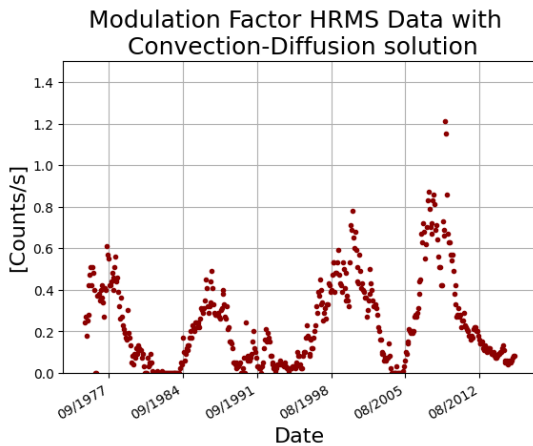


Figure 51: HRMS station. Modulation factor with Convection-Diffusion using Burguer and Potgieter LIS in 2000

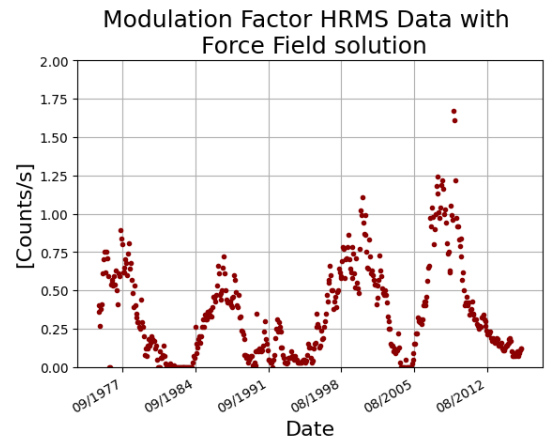


Figure 52: HRMS station. Modulation factor with Force Field using Burguer and Potgieter LIS in 2000

11. APPENDIX

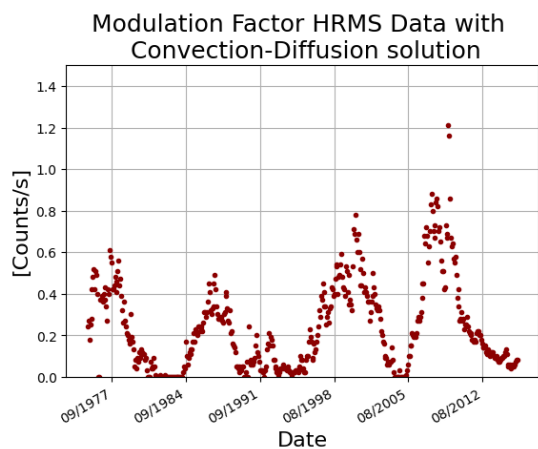


Figure 53: HRMS station. Modulation factor with Convection-Diffusion using Garcia-Munoz, Mason and Simpson LIS in 1975

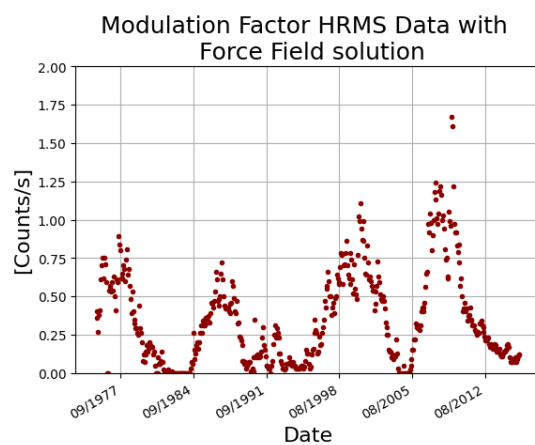


Figure 54: HRMS station. Modulation factor with Force Field using Garcia-Munoz, Mason and Simpson LIS in 1975

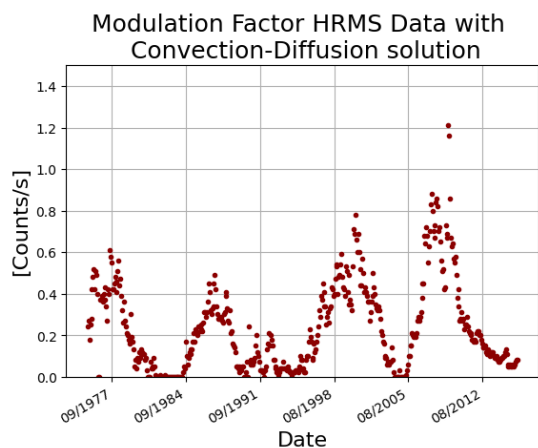


Figure 55: HRMS station. Modulation factor with Convection-Diffusion using Ghelfi, Barao, Derome and Maurin LIS in 2017

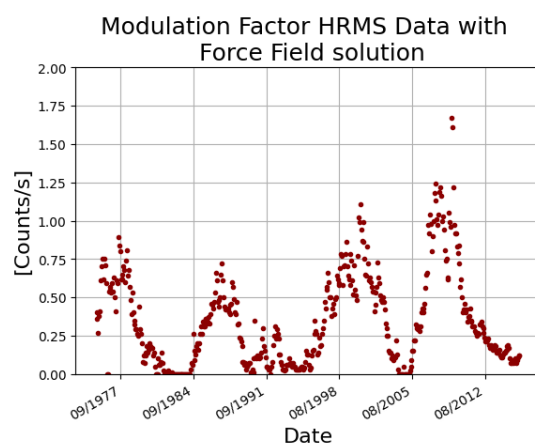


Figure 56: HRMS station. Modulation factor with Force Field using Ghelfi, Barao, Derome and Maurin LIS in 2017

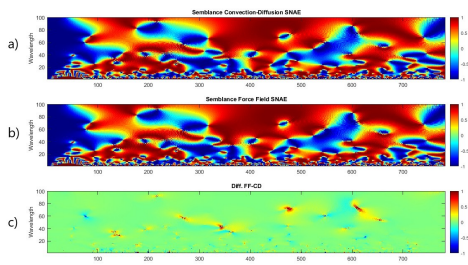


Figure 57: SNAE Station a) Semblance between Modulation Factor using Convection-Diffusion with Lagner, Potgieter and Webber LIS in 2003 vs Sunspot data. b) Semblance between Modulation Factor using Force Field with Lagner, Potgieter and Webber LIS in 2003 vs Sunspot data. c) Difference between the two previous semblances.

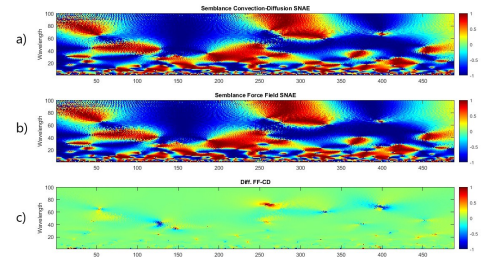


Figure 58: SNAE Station a) Semblance between Modulation Factor using Convection-Diffusion with Lagner, Potgieter and Webber LIS in 2003 vs Mean Magnetic Field data. b) Semblance between Modulation Factor using Force Field with Lagner, Potgieter and Webber LIS in 2003 vs Mean Magnetic Field data. c) Difference between the two previous semblances.

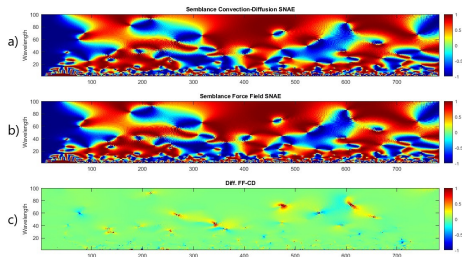


Figure 59: SNAE Station a) Semblance between Modulation Factor using Convection-Diffusion with Burguer and Potgieter LIS in 2000 vs Sunspot data. b) Semblance between Modulation Factor using Force Field with Burguer and Potgieter LIS in 2000 vs Sunspot data. c) Difference between the two previous semblances.

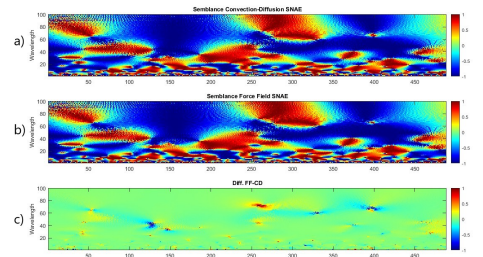


Figure 60: SNAE Station a) Semblance between Modulation Factor using Convection-Diffusion with Burguer and Potgieter LIS in 2000 vs Mean Magnetic Field data. b) Semblance between Modulation Factor using Force Field with Burguer and Potgieter LIS in 2000 vs Mean Magnetic Field data. c) Difference between the two previous semblances.

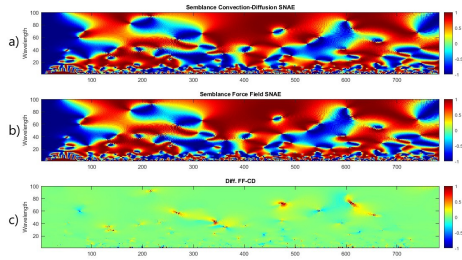


Figure 61: SNAE Station a) Semblance between Modulation Factor using Convection-Diffusion with Garcia-Munoz, Mason and Simpson LIS in 1975 vs Sunspot data. b) Semblance between Modulation Factor using Force Field with Garcia-Munoz, Mason and Simpson LIS in 1975 vs Sunspot data. c) Difference between the two previous semblances.

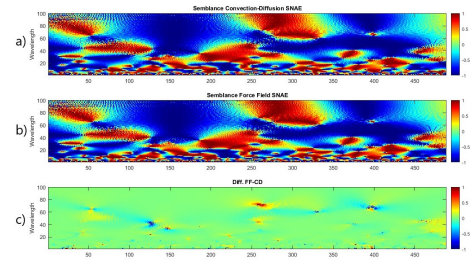


Figure 62: SNAE Station a) Semblance between Modulation Factor using Convection-Diffusion with Garcia-Munoz, Mason and Simpson LIS in 1975 vs Mean Magnetic Field data. b) Semblance between Modulation Factor using Force Field with Garcia-Munoz, Mason and Simpson LIS in 1975 vs Mean Magnetic Field data. c) Difference between the two previous semblances.

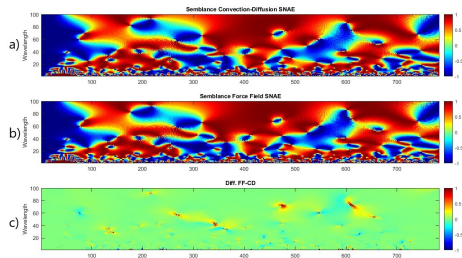


Figure 63: SNAE Station a) Semblance between Modulation Factor using Convection-Diffusion with Ghelfi, Barao, Derome and Maurin LIS in 2017 in 2017 vs Sunspots data. b) Semblance between Modulation Factor using Force Field with Ghelfi, Barao, Derome and Maurin LIS in 2017 in 2017 vs Sunspots data. c) Difference between the two previous semblances.

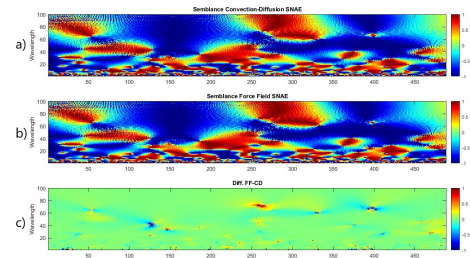


Figure 64: SNAE Station a) Semblance between Modulation Factor using Convection-Diffusion with Ghelfi, Barao, Derome and Maurin LIS in 2017 in 2017 vs Mean Magnetic Field data. b) Semblance between Modulation Factor using Force Field with Ghelfi, Barao, Derome and Maurin LIS in 2017 vs Mean Magnetic Field data. c) Difference between the two previous semblances.